Electric tuning and switching of the resonant response of nanoparticle arrays with liquid crystals

Journal of Applied Physics

Electric tuning and switching of the resonant response of nanoparticle arrays with liquid crystals

Cite as: J. Appl. Phys. **131**, 083101 (2022); https://doi.org/10.1063/5.0079016
Submitted: 17 November 2021 • Accepted: 20 January 2022 • Published Online: 22 February 2022

Erik A. P. van Heijst, Stan E. T. ter Huurne, Jeroen A. H. P. Sol, et al.

Journal of Applied Physics ARTICLE scitation.org/journal/jap

Electric tuning and switching of the resonant response of nanoparticle arrays with liquid crystals

Cite as: J. Appl. Phys. **131**, 083101 (2022); doi: 10.1063/5.0079016
Submitted: 17 November 2021 · Accepted: 20 January 2022 ·
Published Online: 22 February 2022

View Online Export Citation CrossMark

Erik A. P. van Heijst,[1,2,a)] Stan E. T. ter Huurne,[1] Jeroen A. H. P. Sol,[2] Gabriel W. Castellanos,[1] Mohammad Ramezani,[1] Shunsuke Murai,[1,3] Michael G. Debije,[2] and Jaime Gómez Rivas[1,4,b)]

AFFILIATIONS

[1]Department of Applied Physics and Eindhoven Hendrik Casimir Institute, Eindhoven University of Technology, P.O. Box 513, 5600 MB Eindhoven, The Netherlands
[2]Department of Chemical Engineering and Chemistry, Laboratory of Stimuli-Responsive Functional Materials and Devices, Eindhoven University of Technology, P.O. Box 513, 5600 MB Eindhoven, The Netherlands
[3]Department of Material Chemistry, Graduate School of Engineering, Kyoto University, Nishikyo-ku, Kyoto 615-8510, Japan
[4]Institute for Complex Molecular Systems, Laboratory of Macromolecular and Organic Chemistry, Eindhoven University of Technology, 5600 MB Eindhoven, The Netherlands

Note: This paper is part of the Special Topic on Metasurfaces for Photonic Devices.
[a)]**Electronic mail:** erik344@protonmail.com
[b)]**Author to whom correspondence should be addressed:** j.gomez.rivas@tue.nl

ABSTRACT

We report on the design, fabrication, and analysis of a tunable device combining nanoparticle arrays that support collective surface lattice resonances (SLRs) with liquid crystals (LCs). The optoelectronic tunability of the nematic LC and the dependency of sharp SLRs on the refractive index of the environment are exploited to achieve spectral tunability. This tunability is electrically controlled by switching between planar and homeotropic states in the LC, which allows for a rapid and reversible tuning of the SLR wavelength with a large degree of control. This device also offers the possibility to switch "on" and "off" the presence of a quasi-guided mode in the indium tin oxide electrode. The manipulation of these resonances with an external parameter can be used to expand the functionalities of plasmonic metasurface devices.

I. INTRODUCTION

Plasmonic resonances in metallic nanoparticles, or localized surface plasmon resonances (LSPRs), have created a myriad of possibilities, such as nanolasers,[1] extremely sensitive nanosensors for biosensing applications,[2,3] and improved photonic devices.[4–6] At resonance, free electrons in the metallic nanoparticles coherently oscillate in response to an external oscillating electromagnetic field, leading to efficient light scattering and an increased electric field intensity in close proximity to the particles. The increased electric field intensity and light scattering also lead to increased light absorption by the particles, causing the low Q-factor associated with LSPRs. A way to create resonances with a high Q-factor is to arrange the nanoparticles periodically in an array. In such nanoparticle arrays, the LSPRs of the individual particles can couple to in-plane diffraction orders, Rayleigh anomalies (RAs), creating surface lattice resonances (SLRs). SLRs are hybrid plasmonic–photonic modes that exhibit large enhancements in the electric field intensity, despite being delocalized with respect to the individual nanoparticles.[7–9] The plasmonic and photonic character of SLRs is controlled by the parameters of the array, i.e., the particle size that defines the resonant energy of the LSPRs, and the period of the array that defines the energy of the RAs. Depending on the detuning between the LSPRs and the RAs, the prevalent behavior in SLRs is either more photonic or plasmonic.[10] Periodic arrays of

metallic nanoparticles have thus become a favorable type of optical cavity due to their relative ease of fabrication and the ability to tailor resonances through customization of the size of the individual particles and the spacing between them.[10,11]

An enduring ambition in the field of plasmonics and cavity photonics is the active control over the cavity resonances by tuning external parameters. Since SLRs in nanoparticle arrays strongly depend on the refractive index of the environment, liquid crystals (LCs) could offer opportunities for the active control of their resonant response. LCs are materials that combine properties typically associated with both liquid and solid phases: they flow under gravity, yet the constituent molecules ("mesogens") self-assemble into ordered systems. One of the many salient properties of LCs is their birefringence, attributable to a specific orientation of the anisotropic molecules. Moreover, the ability to flow like a liquid allows for control over their orientation and thus the birefringence (and refractive index) of the LC medium. A Fréedericksz phase transition can be induced with an electric potential, where the orientation of the mesogens are quickly and reversibly modified, effectuating local changes in the birefringence of the LC medium.[12,13] Large-area reorientation of the mesogens has been used before to create "smart windows" with electrically addressable light transmittance characteristics.[14,15] The potential of liquid crystals to actively control resonances in metallic nanostructures has already been demonstrated for single nanoparticles supporting LSPRs,[16–20] thin metallic films supporting propagating surface plasmon polaritons (SPPs),[21,22] metasurfaces,[23–31] metallic nanohole arrays,[32] and metallic nanoparticle arrays.[33,34] The wavelength resonance shift resulting from the tuning of LC properties is in most works limited (∼10 nm) and do not involve SLRs, with the exception of Ref. 34, where the tuning of SLRs with LCs and using temperature as the external stimulus is reported. Other methods for creating tunable metasurfaces include fabrication on mechanically reconfigurable substrates,[35,36] using phase change materials,[37] or electrical gating.[38,39] Advantages of LCs over these other options is their wide commercial availability at relatively low cost, the straightforward incorporation into devices, and the absence of optical losses.

In this paper, we report on the electrical tuning of SLRs using LCs. Compared to temperature stimulated switching of LCs, electrical switching is fast and can precisely control the state of the LC in a wider refractive index range. The investigated device consists of an array of aluminum nanoparticles or nanorods fabricated on a transparent indium tin oxide (ITO) electrode with an LC layer on top. Both numerical and experimental methods are employed to study the effect on the optical extinction dispersion (defined as $1 - T$, where T is the transmittance) when the alignment of the LC is changed. We report on a shift in SLR wavelength with a magnitude similar to the resonance width as a result of changing the alignment of the LC. Furthermore, under illumination of TE-polarized light, the device exhibits a quasi-guided mode (QGM) in the ITO layer, which can be switched "on" and "off" by alternating between the alignment states of the LC. The SLR tunability offered by this device could be employed to realize tunable nanolasers or to improve plasmonic sensors.[10,11]

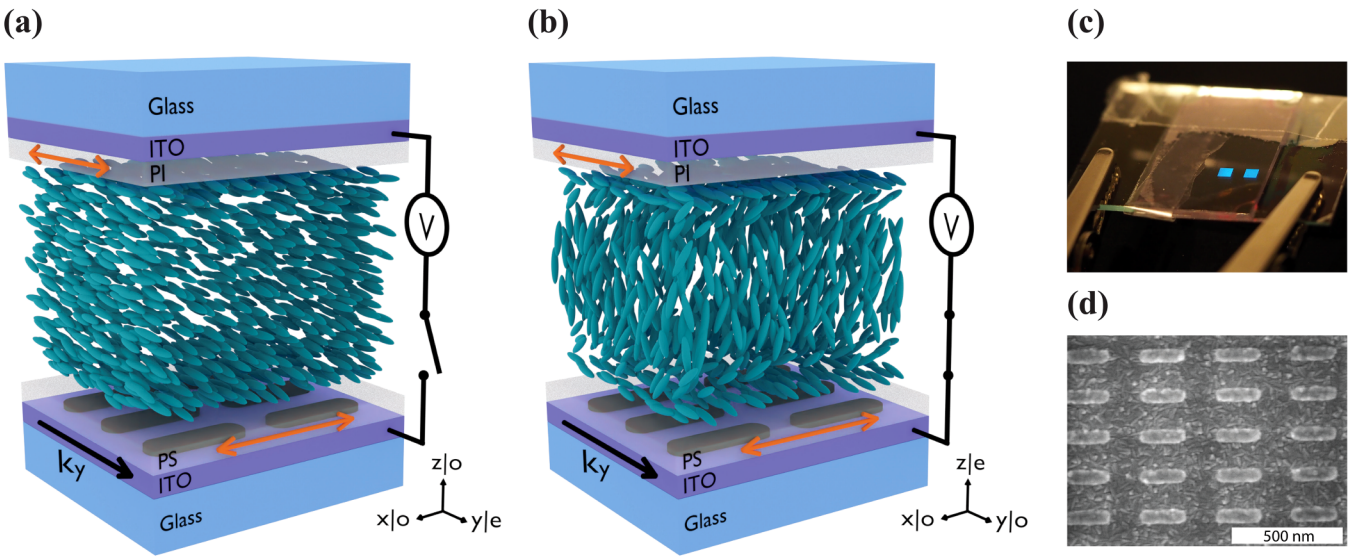

FIG. 1. (a) Schematic representation of the device with planar LC. The device consists of a glass substrate coated with ITO with a nanoparticle array fabricated on top and covered by a PS alignment layer. The LC layer is held in place on top of the PS by a second glass substrate coated with ITO and a PI alignment layer. The rubbing directions of the alignment layers are indicated by the orange double headed arrows. The extraordinary optical axis is parallel to the LC alignment, which is in this case along the y axis. (b) Schematic representation of the same device under application of an electric potential and displaying a homeotropic LC. (c) Photograph of two devices shown as the two squares of arrays with different nanorod sizes but equal array pitches. The angle at which the photo was taken allowed for the diffraction of blue wavelengths to enter the camera, hence the color of the particle arrays. (d) Scanning electron microscope image of the particle array with nanorod dimensions $L_x = 200$, $L_y = 60$, and $L_z = 20$ nm, and array pitches $a_x = 340$ and $a_y = 180$ nm. It is noted that crystalline grains appear on the surface of the ITO film.

II. DEVICE PREPARATION AND CHARACTERIZATION

The design of a device capable of tuning the SLRs in an array of aluminum nanorods is depicted in Figs. 1(a) and 1(b) with the LC in planar and homeotropic alignment states, respectively. The mesogens are aligned along the short axis of the nanorods in the planar LC, while in the homeotropic LC, the mesogens are aligned perpendicular to the substrate. The refractive index tensors for the planar ($\mathbf{n_p}$) and homeotropic ($\mathbf{n_h}$) states are

$$\mathbf{n_p} = \begin{bmatrix} n_o & 0 & 0 \\ 0 & n_e & 0 \\ 0 & 0 & n_o \end{bmatrix}, \quad \mathbf{n_h} = \begin{bmatrix} n_o & 0 & 0 \\ 0 & n_o & 0 \\ 0 & 0 & n_e \end{bmatrix}, \tag{1}$$

where n_o and n_e are the refractive indices associated with the ordinary and extraordinary optical axes. A change from planar to homeotropic alignment, therefore, results in a change in the refractive index ($\Delta n \approx 0.2$) along the y axis from n_e to n_o, as well as a change along the z axis from n_o to n_e.

The device is a cell consisting of two substrates glued together. The cell is built by coating a glass substrate with an ∼130 nm indium tin oxide (ITO) layer, which acts as a transparent electrode upon which the particle array was fabricated (see the Experimental section). Subsequently, an ∼40 nm thick polystyrene (PS) alignment layer was deposited via spin coating on top of the array and mechanically rubbed to induce LC alignment. A second substrate is coated with ITO and an ∼30 nm polyimide (PI) alignment layer, which is rubbed mechanically in a direction perpendicular to the rubbing direction of the PS alignment layer, as indicated by the double-headed orange arrows in Figs. 1(a) and 1(b). This perpendicular arrangement of the alignment layers is necessary due to the parallel alignment of the LC to the rubbing direction of PI but its perpendicular alignment to the rubbing direction of PS.[40] A planar nematic phase of the LC is, therefore, only obtainable when the PI is rubbed in a direction perpendicular to that of PS. Two different alignment layer materials are used since PI cannot be removed with organic solvents but is still a prominent alignment material. The solubility of PS in organic solvents enables the reuse of the particle array for several experiments, whose fabrication process is time consuming. A device combining one PS alignment layer with one PI alignment layer was thus used to form a device that was reusable and of the best quality with respect to the homogeneity of the LC layer. The two substrates are glued together using UV-curable glue containing spacer beads that ensure a cell gap of ∼10 μm. Droplets of the LC mixture are deposited close to the cell gap and drawn into the cell by capillary forces. In the nematic phase at room temperature, the extraordinary optical axis orients parallel to the alignment direction. The Fréedericksz transition from planar to homeotropic is induced by applying an electric potential across the ITO coated substrates via attached alligator clips [see Fig. 1(c)].

Two arrays were investigated with nanorods of different sizes arranged in a rectangular lattice with periods $a_x = 340$ and $a_y = 180$ nm along the x and y directions, respectively. In the first array, the length of the nanorods was $L_x = 200$ nm, while the width and the height were $L_y = 60$ and $L_z = 20$ nm, respectively. A scanning electron microscope (SEM) image of this array, which shall henceforth be referred to as "Array S," is shown in Fig. 1(d). The second array consisted of longer and wider nanorods with dimensions $L_x = 220$, $L_y = 70$, and $L_z = 20$ nm, referred to as "Array L." Figure 2(a) displays a schematic top view of the nanorod array with the mesogens on top in a planar alignment. The arrow indicates the polarization direction of an incident TM-polarized plane wave. Figure 2(b) shows the extinction dispersion of Array S with the LC in planar alignment under TM polarization obtained by numerical simulations (left panel) using the finite-difference time-domain (FDTD) method (see the Experimental section), and the experimental measurements (right panel) obtained using Fourier plane imaging (see the Experimental section as well). There are Fabry–Pérot oscillations present in the measurements due to reflections in the cell consisting of the two substrates; however, the extinction of the SLR is sufficiently large to easily resolve it.

The dispersion of the SLR is calculated and plotted in Fig. 2(b) with a dotted curve. To model this dispersion, we consider a coupled oscillator model that describes the radiative coupling between the LSPRs in the individual nanoparticles and the RAs supported by the array (see the supplementary material). In this coupled oscillator model, one oscillator is represented by the energy of the LSPRs and other two by the energies of the first two degenerate diffraction orders, i.e., the diffraction orders perpendicular to the incident wave vector, given by[41]

$$E_p(k_{y,i})^2 = \left(\frac{\hbar c}{n_e}\right)^2 \left[(k_{y,i})^2 + \left(\frac{2\pi}{a_x}\right)^2\right], \tag{2}$$

where E_p denotes the energies of the in-plane diffracted orders, i.e., the RAs, for the LC in the planar alignment and $k_{y,i}$ is the incident wave vector in the birefringent medium. The refractive index for the planar LC is approximated as n_e based on the dominant field component of the electric fields of the SLR. For the SLR excited with TM polarization, this dominant field component is along the y direction, as can be appreciated in the simulations at $k_y = 0$ and 2.1 eV in Fig. 2(c). The modulus of total field amplitude enhancement (left panel) and the modulus of the y-field component $|E_y|$ (right panel) are displayed in the x–z plane at the location indicated by the red-dashed line in Fig. 2(a). In particular, the field resident in the LC layer—above the gray line in Fig. 2(c)—is almost entirely polarized along the y direction. The difference in amplitude between simulations and experiment can be attributed to the rough surface of the ITO, imperfections in the fabricated nanorods [as can be seen in the SEM image of Fig. 1(d)], and the different illumination conditions. The LC layer is approximated in the simulations to be a semi-infinite medium and the illumination is a perfect plane wave; in the experiments, the entire cell, i.e., with an extra ITO coated glass substrate, is illuminated with a white light source.

For TE polarization, indicated by the arrow in the schematic top view of Fig. 2(d), the extinction dispersion is simulated and measured as shown in the left and right panels of Fig. 2(e). The results show two dispersive resonances around 2 and 2.2 eV at $k_y = 0$ that are identified as an SLR and a quasi-guided mode, respectively.[42] A custom smoothing function, based on the fast Fourier transform (FFT), was used in the measurements to filter

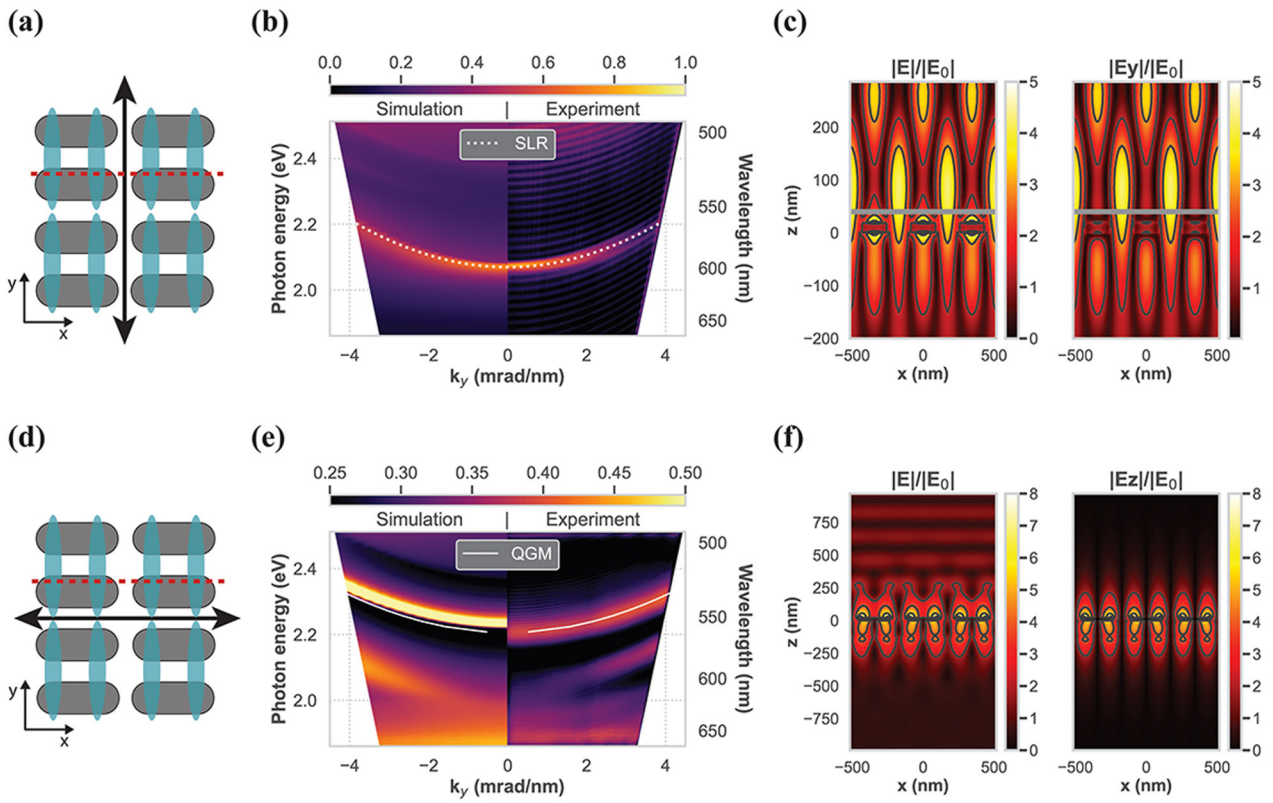

FIG. 2. (a) Schematic representation of the TM polarization (arrow) with respect to the nanorods in the array (gray particles) and the planar alignment of the LC mesogens (blue ellipses). (b) Simulated (left panel) and measured (right panel) extinction dispersion of the Array S device with planar LC alignment under TM-polarized illumination. The SLR, calculated with the coupled oscillator model, is indicated with the white dotted curve. The experimental extinction has been multiplied by a factor 2 to increase the contrast of the SLR over the background. In order to match the simulations to the measurement, the period a_x is adjusted to 344 nm. (c) x–z cross section of the total electric field (left) and the y-field component of the field (right) at the SLR energy calculated in three unit cells of the array at the position of the red-dashed line in (a), and for normal incidence from the top at 2.07 eV. The LC layer is above the gray horizontal line, which is where the majority of the electric field resides. (d) Schematic representation of the TE polarization with respect to the particles in the array and the planar alignment of the LC molecules. (e) Simulated (left panel) and measured (right panel) extinction dispersion of the Array L device with planar LC alignment under TE-polarized illumination. The quasi-guided mode (QGM) in the ITO layer is indicated by the solid-white curve. The extinction of the simulated quasi-guided mode is saturated to increase SLR visibility. (f) x–z cross section of the total electric field and the z-field component at the quasi-guided mode energy calculated in three unit cells of the array at the position of the red-dashed line in (d), and for normal incidence from the top at 2.23 eV. The dominant field component in the case of the quasi-guided mode is the z-component.

out the Fabry–Pérot oscillations. The filter was necessary due to the low contrast between the Fabry–Pérot oscillations and the resonances of the array. The SLR for TE polarization is "dark," meaning that the optical extinction is reduced by lowering k_y, eventually vanishing at $k_y = 0$. The origin of this behavior is in the field symmetry of the scattered wave by $3\lambda/2$ LSPR along the long nanorod axis,[43] which reduces the coupling to the radiation continuum at normal incidence.[44] The quasi-guided mode occurs as a result of the grating coupling of the incident wave by the periodic array in the high refractive index layer defined by the ITO electrode. To model the quasi-guided mode, the device can be approximated as a three-layer system, with a glass bottom layer ($n = 1.515$), ITO middle layer ($n \approx 1.8$), and an effective top layer consisting of both the thin PS alignment layer ($n \approx 1.6$) and LC layer ($n_e = 1.73$, $n_o = 1.52$).[45,46] From the simulated fields at $k_y = 0$ and 2.23 eV, shown in Fig. 2(f) at the location indicated by the red-dashed line in Fig. 2(d), it is apparent that the dominant field component for TE incident polarization is in the z direction along which the refractive index of the LC is n_o. This refractive index is low enough compared to the refractive index of ITO for supporting the guided wave. The dispersion of this quasi-guided mode can be calculated using the waveguide and grating equations[47] (see the supplementary material) and is displayed in Fig. 2(e) as a solid-white curve.

III. LIQUID CRYSTAL TUNING OF SLR AND SWITCHING OF QUASI-GUIDED MODES

The effect of electrically tuning the LC alignment on the SLR wavelength was investigated by measuring the extinction dispersion of the device both without and with an electric potential applied. The electric potential was applied as an AC electric field using an

arbitrary function generator and amplifier with an amplitude of 75 V_{pp} at a frequency of 1 kHz. AC is preferred over DC as the latter can cause heating close to the substrate, which negatively impacts the LC alignment.[48,49] The largest SLR shift for TM polarization is obtained with Array S [Fig. 3(a)]. The results for Array L can be found in the supplementary material. The influence of the particle size on the shift magnitude stems from the hybrid plasmonic–photonic nature of the SLR. SLRs with a larger photonic character are more sensitive to changes in the refractive index of the surroundings than SLRs with a plasmonic character. This behavior is because an SLR with a large photonic character is associated with a higher degree of field delocalization, which is more influenced by the LC layer.[10] A large scattering cross section of the nanorods, induced by their plasmonic character, is necessary to avoid the suppression of the SLR due to the high index contrasts between the multiple layers in the system.[50] The maximum shift of the SLR is, therefore, achieved for a system where the SLR is sufficiently photonic to respond optimally to the changes in refractive

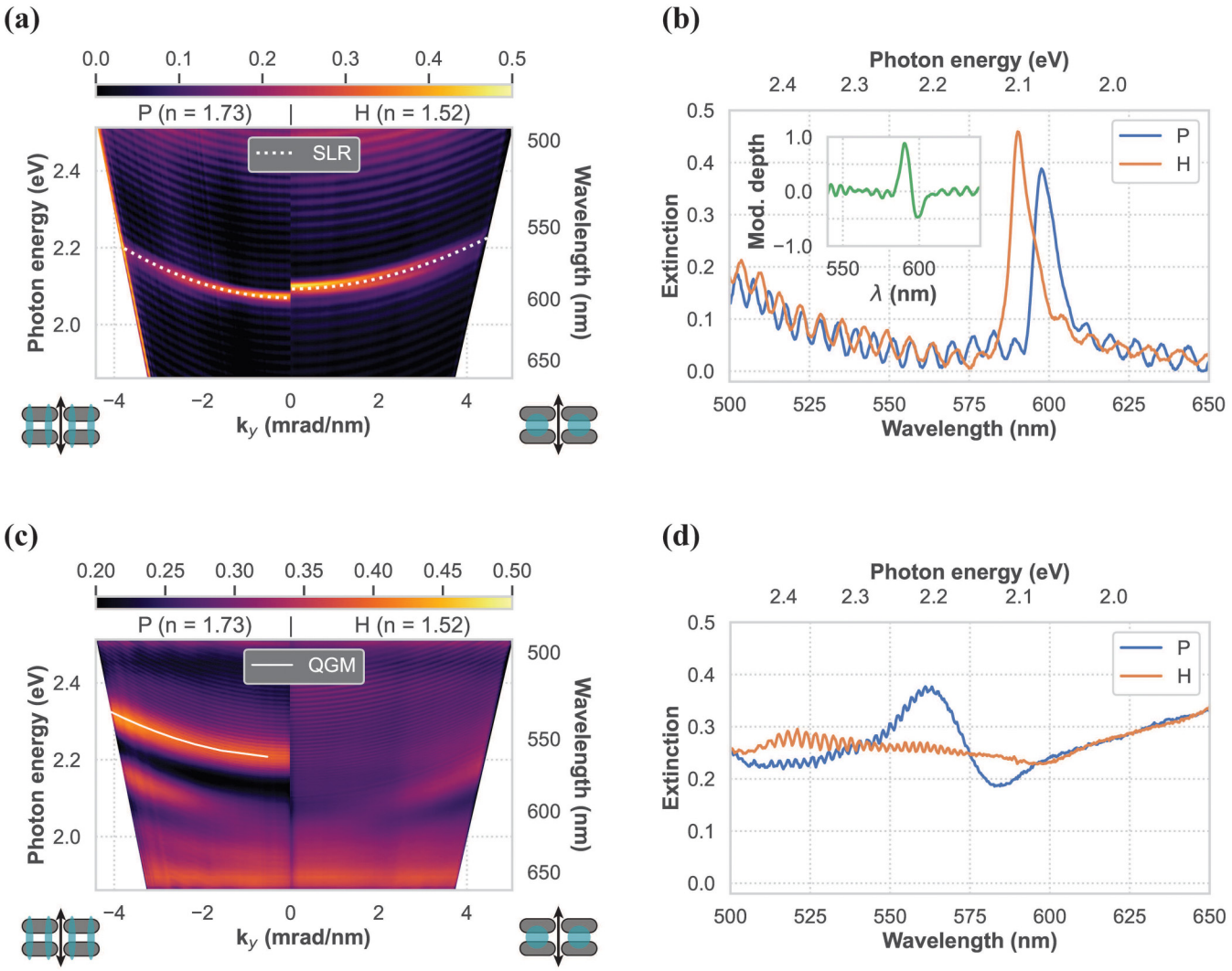

FIG. 3. (a) Extinction dispersion of the Array S device with the LC in planar (P) (left panel) and homeotropic (H) alignments (right panel) for TM-polarized light. The white-dashed curves show the SLR dispersion calculated with the coupled oscillator model. The insets illustrate the TM polarization (arrow) with respect to the particles in the array (gray areas) and the alignment of the LC mesogenes (blue ellipses/circles). (b) Extinction at $k_y = 0$ for both LC alignments. The asymmetric modulation depth is shown in the inset, with a maximum of 88.2% and a minimum of 47.5%. (c) Extinction dispersion of the Array L device with the LC in planar (left panel) and homeotropic alignments (right panel) for TE-polarized light. The solid-white curve indicates the quasi-guided mode in ITO. Similar to (a), the insets show the polarization with respect to array and LC alignment. (d) Extinction of the Array L device at $k_y = 0$ for both LC alignments showing the presence of the quasi-guided mode only in the case of planar LC alignment.

index of the LC but still has a plasmonic character to be present in both LC states. The measured SLR shift amounted to $\Delta\lambda = 7.44$ nm ($\Delta E = 26.2$ meV), which is ≈2.7 times less than the $\Delta\lambda = 19.6$ nm ($\Delta E = 71.6$ meV) shift obtained from simulations (available in the supplementary material). The most probable explanation for this discrepancy is twofold: first, the homeotropic state does not fully correspond to the n_o owing to the mesogens not being perfectly symmetrical rods. Second, a characteristic of the Fréedericksz transition is a gradient from planar to homeotropic in close proximity to the alignment layer [visible in Fig. 1(b)], resulting from the competition between the applied electric field and the anchoring strength of the LC to the alignment layer.[51] This gradient influences the effective refractive index close to the ITO coated substrates, and, thus, especially influences the SLR of the ITO-bound particle arrays. Both of these reasons reduce the effective birefringence of the LC in the proximity of the particle arrays.

An interesting property is the modulation depth of the SLR, i.e., the overlap between the SLRs associated with both LC states. The modulation depth is calculated as $(\mathcal{E}_H - \mathcal{E}_P)/\max(\mathcal{E}_H)$, where $\mathcal{E}_P$ and $\mathcal{E}_H$ are the optical extinction for planar and homeotropic LC, respectively. The extinctions at $k_y = 0$ for both LC alignments are shown in Fig. 3(b), while the modulation depth is shown in the

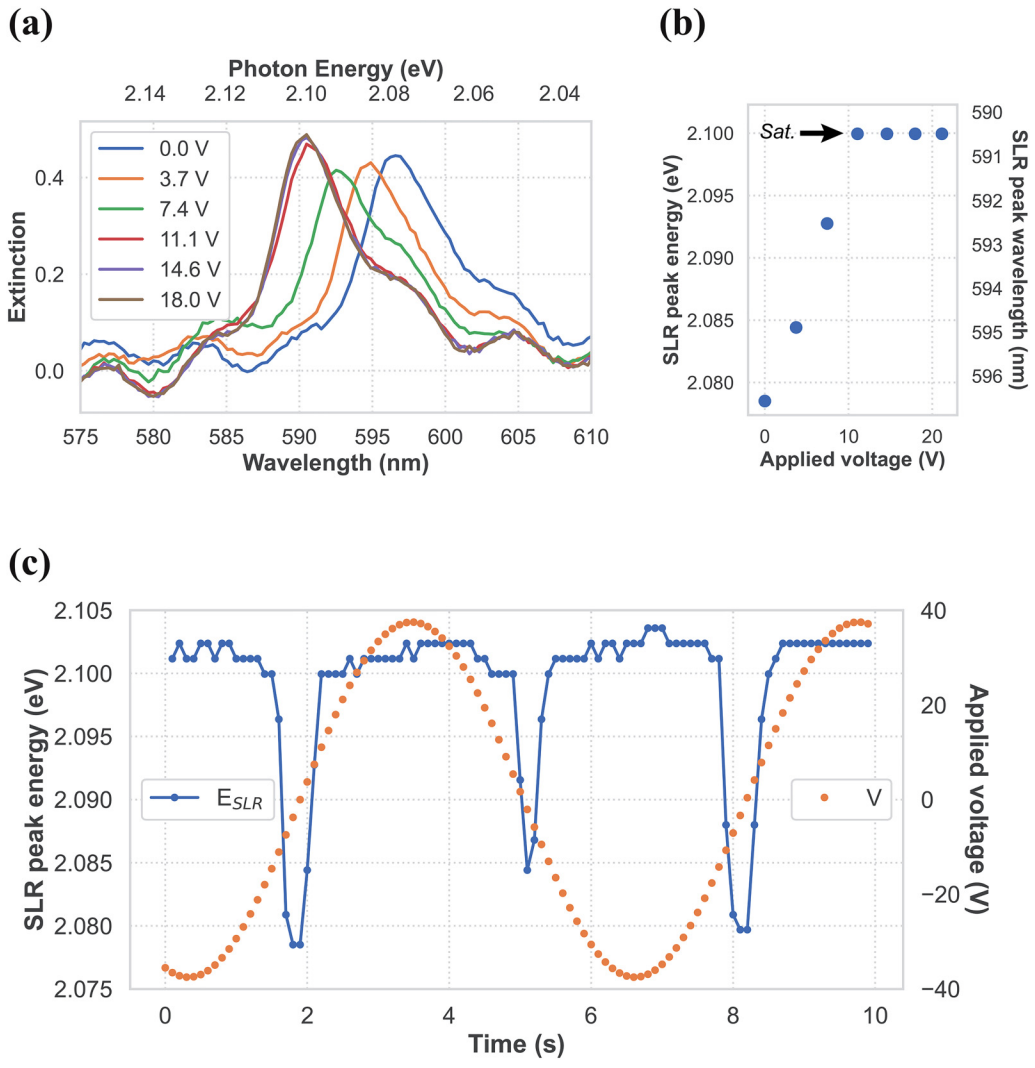

FIG. 4. (a) Optical extinction of Array S measured at $k_y = 0$ for six different voltages. The SLR does not change for higher voltages than 11.0 V, indicating the saturation point. (b) SLR extinction peak maxima as a function of the applied voltage where the saturation voltage related to the Fréedericksz transition is indicated. (c) Measurement of the SLR extinction peak energy over time under application of a low frequency oscillating electric field. The SLR peak energy is indicated with the blue circles and the solid curve. The orange circles display the applied oscillating electric field.

inset. An asymmetric modulation depth is obtained, owing to the asymmetric Fano line shape of SLRs and different amplitudes, with a maximum of ∼90% and a minimum of ∼50%.

Switching the LC from planar to homeotropic for TE polarization not only results in a shift in the SLR but also the quasi-guided mode in the ITO layer disappears, as can be seen in Fig. 3(c). The latter is a particularly interesting effect since the quasi-guided mode can be switched "on" and "off" by the LC alignment. This phenomenon results from the conditions that lead to waveguiding in a slab.[47] In a three-layer system (top layer–middle layer–bottom layer) with three refractive indices n_1, n_2, and n_3, the condition for a quasi-guided mode is met when $n_2 \sin(\theta_d) > n_1, n_3$, where θ_d is the angle of diffraction from the array. In our device, n_2 is the refractive index of the ITO layer, n_3 is the refractive index of the glass, and n_1 is the effective refractive index of alignment layer and LC. The refractive index of the LC is determined mainly by the z-component according to the fields shown in Fig. 2(f), which is n_o for planar alignment and n_e for homeotropic alignment. For planar LC alignment, the condition for quasi-guided modes is satisfied due to the lower n_o. The larger n_e for homeotropic alignment accounts for a reduced contrast between n_2 and n_1, and the condition for a quasi-guided mode is no longer met. The extinction at $k_y = 0$ in Fig. 3(d) further exemplifies that the quasi-guided mode indeed only exists for one alignment of the LC.

Electrical switching of the LC has two main advantages over switching the LC with temperature. First, it allows for quick switching between the planar and homeotropic states on a timescale on the order of milliseconds.[52] The relaxation from homeotropic to planar after the potential is removed takes a couple of seconds at most due to the reorientation of the mesogens influenced by the alignment layers. The second advantage is the possibility to quickly obtain every alignment in between the planar and homeotropic states, enabling a high degree of control of the SLR. To confirm that the ability to actively tune the refractive index of the LC translates to active tuning of the SLR, extinction measurements were performed with a lower AC frequency of 150 mHz. The lower AC frequency allowed for the LC alignment to gradually change in response to a slowly oscillating electric field. The extinction measurements at $k_y = 0$ are shown in Fig. 4(a) at six different electric potentials between the homeotropic and planar LC alignments. These measurements show that, indeed, a significant degree of control can be exerted over the SLRs by tailoring the alignment of the LCs. The position of the SLR peak as a function of applied potential is depicted in Fig. 4(b) in which a saturation associated with a fully realized Fréedericksz transition can be observed at ∼10 V. Figure 4(c) shows three full switching cycles (homeotropic–planar–homeotropic) of the liquid crystal alignment as a function of applied voltage. The peaks in Fig. 4(c) illustrate the switching to planar alignment and back, which takes place within 1 s. Due to the large amplitude of the applied electric field (75 V_{pp}), the LC spends most of the time in the homeotropic alignment state.

IV. CONCLUSIONS

We have designed, fabricated, and measured a device consisting of a particle array topped by a nematic LC. In this device, it is possible to tune the energy of a collective plasmonic resonance or surface lattice resonance (SLR) by changing the refractive index of the LC under an applied electric potential. Since the tuning of the liquid crystal is performed by an applied electric potential, the shift of the SLR is rapid, reversible, and executed with a large degree of control. The experimental SLR energy shift is less than the expected shift obtained from simulations. The most probable explanation for the discrepancy is a gradient from planar to homeotropic in close proximity to the alignment layers and, hence, in close proximity to the nanoparticle array. This device can also switch "on" and "off" quasi-guided modes in the ITO layer used as an electrode by controlling the LC alignment. Active control of resonant systems is important for the realization of tunable devices that can be exploited for light emission, lasing, and in sensing applications.

V. EXPERIMENTAL SECTION

Aluminum nanoparticle arrays were fabricated using electron beam lithography and lift-off processes. First, the resist (ZEP520A) was coated onto an ITO thin film (thickness ∼ 130 nm) on the substrate (Eagle XG, Corning) and prebaked for 3 min at 180 °C. The resist was nanopatterned by electron beam lithography (F7000s-KYT01, Advantest), followed by developing with a developer (ZED-N50). Then, an Al thin film (thickness = 20 nm) was grown on the prepatterned resist on the substrate using electron beam deposition. Finally, a lift-off process was performed with a solvent (ST-120) to remove the excess Al on the resist. There is a 3 nm thick natural oxide layer (Al_2O_3) formed on top of the nanoparticles giving the long-term stability needed for applications.

Substrate pre-treatment for LC cell was performed in two steps: cleaning of the substrate and spin coating with a polymer layer. The substrates used in the LC cell construction (including those with fabricated particle arrays) were cleaned by sonication in a 1:1 v/v 2-propanol to ethanol mixture for 20 min. Both the Bandelin Sonorex Super ultrasonic bath and the Marshall Scientific Branson 2510 ultrasonic cleaner were used for this purpose. After sonication, the substrates were placed in a UV–ozone (both the UVP PR-100 and the Jelight Company UVO Cleaner®) photoreactor to clean any smaller contaminants. Spin coating of the PI alignment layer (Optmer AL-1254 display material purchased from JSR Corp) is done with a Karl Suss RC6 at 5000 rpm for 45 s in order to obtain 30–40 nm layers, after which the PI layers were cured for 90 min at 180 °C in a Heraeus Instruments vacutherm oven at atmospheric pressure. Other spin coating was performed using the Laurell model WS-650MZ-23NPPB. PS (M_w = 200 000 by GPC, purchased from Sigma-Aldrich Inc.) layers were spin coated out of a 1.5 wt% solution in anisole at a speed of 3000 rpm for 60 s to obtain 35–40 nm layers as determined by a Bruker DektakXT® profilometer. After coating, the substrates were placed on a hotplate at 80 °C for 10 min.

Cell fabrication. The PI and PS coated substrates were mechanically rubbed using a rubbing machine, which consists of two main components, the roller and the moving table, each attached to a motor and controlled by a separate controller box. The roller motor is a Bodine Electric Company small motor model type 33A5BEPM 130 V DC and controlled by a Dart Controls micro-drive MD10P. The table motor is an ElectroCraft E288 and

controlled by an Electro-Craft Motomatic II. The substrate is attached to the table using the KNF Laboport lab vacuum pump. UV Sealant 91 from Norland Inc. to which 1 wt% resin spacer beads of Micropearl SP series (purchased from Sekisui Chemical Co., Ltd.) were used to glue the substrates together while maintaining a 10 μm cell gap. The cell thickness was confirmed using a PerkinElmer Lambda 750 UV/VIS/NIR spectrophotometer and fitting the measured Fabry–Pérot oscillations in the wavelength range of 1000–2000 nm to an Airy distribution, yielding a value for the cell gap. The cell was then filled with LC mixture E7 purchased from Merck KGaA, Darmstadt Germany.

Electric potential was applied to the cell using a AIM-TTi TG1010 programmable 10 MHz DDS Function Generator combined with a Falco Systems WMA-300 High Voltage Amplifier DC −5 MHz.

Finite-difference time-domain simulations were performed using Ansys Lumerical 2021 R1.4 Finite Difference IDE. The LC layer is approximated as a semi-infinite medium, as is the glass substrate. The 130 nm ITO layer, whose optical constants are obtained from ellipsometry, as well as a 40nm PS layer are included in the simulation. The Al nanorod is designed as a rectangle with rounded corners, whose optical constants were also obtained from ellipsometry. The boundary conditions for extinction dispersion simulations were Bloch-periodic boundary conditions in the transverse directions and perfect matching layers (PMLs) in the z direction with a standard PML profile consisting of 20 layers. An unstructured mesh was used by adding an overriding high resolution mesh (2 nm step size in each direction) directly in the nanorod.

Fourier plane imaging measurements are performed using a low-power white light beam from a tungsten–halogen lamp focused onto the sample with a 40x objective (NA = 0.6). The transmitted light through the sample is collected by another 60x objective (NA = 0.7), and the back focal plane of this objective is imaged at the entrance slit of a spectrometer. The imaging spectrometer retrieves the transmission spectra as a function of angle. These measurements can be plotted in a dispersion diagram, representing the optical extinction as a function of the photon energy and the wave vector parallel to the surface, i.e., $k_{\parallel} = \frac{2\pi}{\lambda}\sin(\theta)$. The related extinction is defined as $1 - T/T_{\mathrm{REF}}$, where T is the transmission through the sample and T_{REF} is a reference transmission measured through the sample on a location without a particle array.

SUPPLEMENTARY MATERIAL

See the supplementary material for the equations pertaining to the Coupled Oscillator Model for SLR calculation and the equations for the quasi-guided modes. Furthermore, the supplementary material contains the FDTD simulations of the measurements displayed in Fig. 3 and the extinction dispersion measurements of the devices with orthogonal polarizations to those described in this paper.

ACKNOWLEDGMENTS

This work was financially supported by the Nederlandse Organisatie voor Wetenschappelijk Onderzoek (NWO) (Vici Grant No. 680-47-628). SM acknowledges support from the Joint Research Project (JPJSBP120219920) from JSPS, Japan. The authors would like to thank J. Beeckman for discussions.

AUTHOR DECLARATIONS

Conflict of Interest

The authors have no conflicts of interest to disclose.

DATA AVAILABILITY

The data that support the findings of this study are available from the corresponding author upon reasonable request.

REFERENCES

[1]J. Y. Suh, C. H. Kim, W. Zhou, M. D. Huntington, D. T. Co, M. R. Wasielewski, and T. W. Odom, "Plasmonic bowtie nanolaser arrays," Nano Lett. **12**, 5769–5774 (2012).
[2]J. N. Anker, W. P. Hall, O. Lyandres, N. C. Shah, J. Zhao, and R. P. Van Duyne, "Biosensing with plasmonic nanosensors," Nat. Mater. **7**, 442–453 (2008).
[3]A. V. Kabashin, P. Evans, S. Pastkovsky, W. Hendren, G. A. Wurtz, R. Atkinson, R. Pollard, V. Podolskiy, and A. V. Zayats, "Plasmonic nanorod metamaterials for biosensing," Nat. Mater. **8**, 867–871 (2009).
[4]H. A. Atwater and A. Polman, "Plasmonics for improved photovoltaic devices," Nat. Mater. **9**, 205–213 (2010).
[5]G. Lozano, D. J. Louwers, S. R. Rodríguez, S. Murai, O. T. Jansen, M. A. Verschuuren, and J. G. Rivas, "Plasmonics for solid-state lighting: Enhanced excitation and directional emission of highly efficient light sources," Light Sci. Appl. **2**, e66 (2013).
[6]G. Lozano, S. R. Rodriguez, M. A. Verschuuren, and J. G. Rivas, "Metallic nanostructures for efficient led lighting," Light Sci. Appl. **5**, e16080 (2016).
[7]V. G. Kravets, A. V. Kabashin, W. L. Barnes, and A. N. Grigorenko, "Plasmonic surface lattice resonances: A review of properties and applications," Chem. Rev. **118**, 5912–5951 (2018).
[8]W. Wang, M. Ramezani, A. I. Väkeväinen, P. Törmä, J. G. Rivas, and T. W. Odom, "The rich photonic world of plasmonic nanoparticle arrays," Mater. Today **21**, 303–314 (2018).
[9]A. D. Utyushev, V. I. Zakomirnyi, and I. L. Rasskazov, "Collective lattice resonances: Plasmonics and beyond," Rev. Phys. **6**, 100051 (2021).
[10]P. Offermans, M. C. Schaafsma, S. R. K. Rodriguez, Y. Zhang, M. Crego-Calama, S. H. Brongersma, and J. Gómez Rivas, "Universal scaling of the figure of merit of plasmonic sensors," ACS Nano **5**, 5151–5157 (2011).
[11]D. Wang, A. Yang, W. Wang, Y. Hua, R. D. Schaller, G. C. Schatz, and T. W. Odom, "Band-edge engineering for controlled multi-modal nanolasing in plasmonic superlattices," Nat. Nanotechnol. **12**, 889–894 (2017).
[12]V. Fréedericksz and A. Repiewa, "Theoretisches und experimentelles zur frage nach der natur der anisotropen flüssigkeiten," Z. Phys. **42**, 532–546 (1927).
[13]V. Fréedericksz and V. Zolina, "Forces causing the orientation of an anisotropic liquid," Trans. Faraday Soc. **29**, 919–930 (1933).
[14]M. G. Debije, "Solar energy collectors with tunable transmission," Adv. Funct. Mater. **20**, 1498–1502 (2010).
[15]J. A. H. P. Sol, G. H. Timmermans, A. J. van Breugel, A. P. H. J. Schenning, and M. G. Debije, "Multistate luminescent solar concentrator 'smart' windows," Adv. Energy Mater. **8**, 1702922 (2018).
[16]J. Müller, C. Sönnichsen, H. Von Poschinger, G. Von Plessen, T. Klar, and J. Feldmann, "Electrically controlled light scattering with single metal nanoparticles," Appl. Phys. Lett. **81**, 171–173 (2002).
[17]P. A. Kossyrev, A. Yin, S. G. Cloutier, D. A. Cardimona, D. Huang, P. M. Alsing, and J. M. Xu, "Electric field tuning of plasmonic response of nanodot array in liquid crystal matrix," Nano Lett. **5**, 1978–1981 (2005).

[18]K. Chu, C. Chao, Y. Chen, Y. Wu, and C. C. Chen, "Electrically controlled surface plasmon resonance frequency of gold nanorods," Appl. Phys. Lett. **89**, 103107 (2006).
[19]P. Evans, G. Wurtz, W. Hendren, R. Atkinson, W. Dickson, A. Zayats, and R. Pollard, "Electrically switchable nonreciprocal transmission of plasmonic nanorods with liquid crystal," Appl. Phys. Lett. **91**, 043101 (2007).
[20]S. Khatua, W.-S. Chang, P. Swanglap, J. Olson, and S. Link, "Active modulation of nanorod plasmons," Nano Lett. **11**, 3797–3802 (2011).
[21]H. Li, S. Xu, Y. Gu, K. Wang, and W. Xu, "Active modulation of wavelength and radiation direction of fluorescence via liquid crystal-tuned surface plasmons," Appl. Phys. Lett. **102**, 051107 (2013).
[22]A. E. Cetin, A. Mertiri, M. Huang, S. Erramilli, and H. Altug, "Thermal tuning of surface plasmon polaritons using liquid crystals," Adv. Opt. Mater. **1**, 915–920 (2013).
[23]J. A. Dolan, H. Cai, L. Delalande, X. Li, A. B. Martinson, J. J. De Pablo, D. López, and P. F. Nealey, "Broadband liquid crystal tunable metasurfaces in the visible: Liquid crystal inhomogeneities across the metasurface parameter space," ACS Photonics **8**, 567–575 (2021).
[24]M. Decker, C. Kremers, A. Minovich, I. Staude, A. E. Miroshnichenko, D. Chigrin, D. N. Neshev, C. Jagadish, and Y. S. Kivshar, "Electro-optical switching by liquid-crystal controlled metasurfaces," Opt. Express **21**, 8879–8885 (2013).
[25]C. Zou, C. Amaya, S. Fasold, A. A. Muravsky, A. A. Murauski, T. Pertsch, and I. Staude, "Multiresponsive dielectric metasurfaces," ACS Photonics **8**, 1775 (2021).
[26]R. Kowerdziej, J. Wróbel, and P. Kula, "Ultrafast electrical switching of nanostructured metadevice with dual-frequency liquid crystal," Sci. Rep. **9**, 20367 (2019).
[27]S. Xiao, U. K. Chettiar, A. V. Kildishev, V. Drachev, I. Khoo, and V. M. Shalaev, "Tunable magnetic response of metamaterials," Appl. Phys. Lett. **95**, 033115 (2009).
[28]A. Komar, Z. Fang, J. Bohn, J. Sautter, M. Decker, A. Miroshnichenko, T. Pertsch, I. Brener, Y. S. Kivshar, I. Staude *et al.*, "Electrically tunable all-dielectric optical metasurfaces based on liquid crystals," Appl. Phys. Lett. **110**, 071109 (2017).
[29]C. Zou, A. Komar, S. Fasold, J. Bohn, A. A. Muravsky, A. A. Murauski, T. Pertsch, D. N. Neshev, and I. Staude, "Electrically tunable transparent displays for visible light based on dielectric metasurfaces," ACS Photonics **6**, 1533–1540 (2019).
[30]J. Sautter, I. Staude, M. Decker, E. Rusak, D. N. Neshev, I. Brener, and Y. S. Kivshar, "Active tuning of all-dielectric metasurfaces," ACS Nano **9**, 4308–4315 (2015).
[31]J. Bohn, T. Bucher, K. E. Chong, A. Komar, D.-Y. Choi, D. N. Neshev, Y. S. Kivshar, T. Pertsch, and I. Staude, "Active tuning of spontaneous emission by Mie-resonant dielectric metasurfaces," Nano Lett. **18**, 3461–3465 (2018).
[32]W. Dickson, G. A. Wurtz, P. R. Evans, R. J. Pollard, and A. V. Zayats, "Electronically controlled surface plasmon dispersion and optical transmission through metallic hole arrays using liquid crystal," Nano Lett. **8**, 281–286 (2008).
[33]J. Li, Y. Ma, Y. Gu, I.-C. Khoo, and Q. Gong, "Large spectral tunability of narrow geometric resonances of periodic arrays of metallic nanoparticles in a nematic liquid crystal," Appl. Phys. Lett. **98**, 213101 (2011).
[34]A. Abass, S. R.-K. Rodriguez, T. Ako, T. Aubert, M. Verschuuren, D. Van Thourhout, J. Beeckman, Z. Hens, J. Gómez Rivas, and B. Maes, "Active liquid crystal tuning of metallic nanoantenna enhanced light emission from colloidal quantum dots," Nano Lett. **14**, 5555–5560 (2014).
[35]H.-S. Ee and R. Agarwal, "Tunable metasurface and flat optical zoom lens on a stretchable substrate," Nano Lett. **16**, 2818–2823 (2016).
[36]X. Zhang, Y. Zhou, H. Zheng, A. E. Linares, F. C. Ugwu, D. Li, H.-B. Sun, B. Bai, and J. G. Valentine, "Reconfigurable metasurface for image processing," Nano Lett. **21**, 8715 (2021).
[37]F. Ding, Y. Yang, and S. I. Bozhevolnyi, "Dynamic metasurfaces using phase-change chalcogenides," Adv. Opt. Mater. **7**, 1801709 (2019).
[38]Y. Yao, R. Shankar, M. A. Kats, Y. Song, J. Kong, M. Loncar, and F. Capasso, "Electrically tunable metasurface perfect absorbers for ultrathin mid-infrared optical modulators," Nano Lett. **14**, 6526–6532 (2014).
[39]Y.-W. Huang, H. W. H. Lee, R. Sokhoyan, R. A. Pala, K. Thyagarajan, S. Han, D. P. Tsai, and H. A. Atwater, "Gate-tunable conducting oxide metasurfaces," Nano Lett. **16**, 5319–5325 (2016).
[40]J. Stöhr and M. Samant, "Liquid crystal alignment by rubbed polymer surfaces: A microscopic bond orientation model," J. Electron Spectrosc. Relat. Phenom. **98**, 189–207 (1999).
[41]G. Vecchi, V. Giannini, and J. G. Rivas, "Shaping the fluorescent emission by lattice resonances in plasmonic crystals of nanoantennas," Phys. Rev. Lett. **102**, 146807 (2009).
[42]S. Murai, M. Verschuuren, G. Lozano, G. Pirruccio, S. Rodriguez, and J. G. Rivas, "Hybrid plasmonic-photonic modes in diffractive arrays of nanoparticles coupled to light-emitting optical waveguides," Opt. Express **21**, 4250–4262 (2013).
[43]L. Novotny, "Effective wavelength scaling for optical antennas," Phys. Rev. Lett. **98**, 266802 (2007).
[44]M. Ramezani, A. Halpin, A. I. Fernández-Domínguez, J. Feist, S. R.-K. Rodriguez, F. J. Garcia-Vidal, and J. G. Rivas, "Plasmon-exciton-polariton lasing," Optica **4**, 31–37 (2017).
[45]V. Tkachenko, G. Abbate, A. Marino, F. Vita, M. Giocondo, A. Mazzulla, F. Ciuchi, and L. D. Stefano, "Nematic liquid crystal optical dispersion in the visible-near infrared range," Mol. Cryst. Liq. Cryst. **454**, 263/[665]–271/[673] (2006).
[46]J. Li, C.-H. Wen, S. Gauza, R. Lu, and S.-T. Wu, "Refractive indices of liquid crystals for display applications," J. Disp. Technol. **1**, 51 (2005).
[47]K. Guo, G. Lozano, M. A. Verschuuren, and J. Gómez Rivas, "Control of the external photoluminescent quantum yield of emitters coupled to nanoantenna phased arrays," J. Appl. Phys. **118**, 073103 (2015).
[48]A. A. F. Froyen, M. Wübbenhorst, D. Liu, and A. P. H. J. Schenning, "Electrothermal color tuning of cholesteric liquid crystals using interdigitated electrode patterns," Adv. Electron. Mater. **7**, 2000958 (2021).
[49]S.-A. Jiang, J.-L. Chang, J.-W. Lin, Y.-S. Zhang, T.-S. Mo, J.-D. Lin, and C.-R. Lee, "Toward full-color tunable chiroptical electrothermochromic devices based on a supramolecular chiral photonic material," Adv. Opt. Mater. **9**, 2001796 (2021).
[50]B. Auguié, X. M. Bendana, W. L. Barnes, and F. J. G. de Abajo, "Diffractive arrays of gold nanoparticles near an interface: Critical role of the substrate," Phys. Rev. B **82**, 155447 (2010).
[51]R. Self, C. Please, and T. Sluckin, "Deformation of nematic liquid crystals in an electric field," Eur. J. Appl. Math. **13**, 1–23 (2002).
[52]V. M. Di Pietro, A. Jullien, U. Bortolozzo, N. Forget, and S. Residori, "Dynamical optical response of nematic liquid crystal cells through electrically driven fréedericksz transition: Influence of the nematic layer thickness," Opt. Express **26**, 10716–10728 (2018).